NEW METHOD FOR PREDICTING LIFETIME OF SEALS FROM COMPRESSION-STRESS RELAXATION EXPERIMENTS

Kenneth T. Gillen, Michael R. Keenan and Jonathan Wise
Sandia National Laboratories, Albuquerque, NM 87185-1407, USA

ABSTRACT

Interpretation of compression stress-relaxation (CSR) experiments for elastomers in air is complicated by (1) the presence of both physical and chemical relaxation and (2) anomalous diffusion-limited oxidation (DLO) effects. For a butyl material, we first use shear relaxation data to indicate that physical relaxation effects are negligible during typical high temperature CSR experiments. We then show that experiments on standard CSR samples (~15 mm diameter when compressed) lead to complex non-Arrhenius behavior. By combining reaction kinetics based on the historic basic autoxidation scheme with a diffusion equation appropriate to disk-shaped samples, we derive a theoretical DLO model appropriate to CSR experiments. Using oxygen consumption and permeation rate measurements, the theory shows that important DLO effects are responsible for the observed non-Arrhenius behavior. To minimize DLO effects, we introduce a new CSR methodology based on the use of numerous small disk samples strained in parallel. Results from these parallel, minidisk experiments lead to Arrhenius behavior with an activation energy consistent with values commonly observed for elastomers, allowing more confident extrapolated predictions. In addition, excellent correlation is noted between the CSR force decay and the oxygen consumption rate, consistent with the expectation that oxidative scission processes dominate the CSR results.

INTRODUCTION

When polymers are placed under constant mechanical strain, the resulting stress will relax with time from a combination of physical and chemical processes [1-3]. The physical processes involve such things as flow of chains and movement of entanglements. For elastomeric (crosslinked) materials in the absence of chemical effects, the physical effects are reversible in the sense that the material will eventually recover its original shape once the mechanical strain is removed. The chemical processes, on the other hand, are irreversible, involving mainly scission and crosslinking effects (breakage and formation, respectively, of covalent bonds). Various stress-relaxation methods, involving primarily tensile and compressive sample loading, have been used for many decades to study and model these effects [1-6]. Our current objective is to derive better methods for estimating the lifetime of elastomeric seals in oxygen-containing environments (e.g., air). Since service lifetimes depend primarily on the decay in compressive force between the seal and its mating surface and since compression stress-relaxation (CSR) techniques [4-6] follow the force for compressively loaded samples, CSR is usually considered to be the most appropriate approach for lifetime predictions of seals and will therefore be used for that purpose in the current study.

DISCLAIMER

When oxidative chemical degradation effects are significant during stress-relaxation experiments, attempts to analyze and model the data are complicated by two phenomena, the need to separate the physical and chemical relaxation processes and the potential presence of anomalous diffusion-limited oxidation (DLO) effects. Various workers have suggested methods for separating physical from chemical effects, including Curro and Salazar [7], Stenberg and Jansson [8], Ito [9] and Murakami, et. al. [10]. In this study, we utilize a method based on the Curro-Salazar approach to show that physical effects are unimportant for the temperatures and times used for probing the chemical effects. Previous work attempting to understand and model DLO effects on stress-relaxation experiments was mainly due to Murakami and co-workers [10-13]. These workers tried to quantitatively model tensile stress-relaxation results versus sample thickness and surrounding oxygen partial pressure using a diffusion-reaction equation that assumed a linear dependence of reaction rate on oxygen concentration. Although this assumption may be valid for very low oxygen partial pressures, it is usually inappropriate under typical application conditions (i.e., air); in their later papers, Murakami, et. al. [14] acknowledge this conclusion. A more general diffusion-reaction model for DLO effects on sheet material was derived by Cunliffe and Davis [15] using a higher-level reaction rate expression based on the classic basic autoxidation scheme [16,17]. Although the bimolecular termination reactions used in the Cunliffe and Davis model are inappropriate for stabilized elastomers, recent work [18,19] indicates that unimolecular termination variations of the basic oxidation scheme give a DLO model essentially identical to that derived by Cunliffe and Davis. Careful studies over the past few years have shown that this general DLO model gives quantitative agreement with experimental results for elastomers aged in both radiation and thermoxidative environments [18-20]. In the current paper, we couple this more general oxidation rate expression with diffusion expressions appropriate to the disk geometry used in most CSR experiments to derive the DLO model appropriate to CSR studies. We use this modeling coupled with experimental results to show that large errors are introduced by DLO effects for typical CSR samples. Finally we introduce a method for eliminating such errors.

EXPERIMENTAL

Compression molded sheets of a commercial, peroxide-cured butyl rubber were obtained from Parker Seal Company (Parker compound B612-70) in two thicknesses (~1 mm and ~2 mm). To prepare the cylindrical samples needed for standard compression stress relaxation experiments, three 12.7 mm diameter disc-shaped samples were cut from the 2 mm thick compression-molded sheets and stacked on top of one another to obtain an unstrained cylinder of 12.7 mm diameter and a typical thickness of 6 mm. To make 2 mm diameter disks, a stainless steel circular die with very thin cutting surfaces was specially prepared. The 2 mm mini-disk samples were cut from the 1-mm thick sheet, so that the ratio of disk diameter to disk thickness was approximately the same as for the standard samples. Since the area of a single 2 mm disk leads to a very small force when compressed, obtaining reasonable CSR force values requires the use of multiple minidisks strained in parallel (the current series of experiments uses 50). To ensure that the 50 mini-disks for a given experiment had similar unstrained thicknesses, they were all cut from a small area of a sheet (~2 cm by 2 cm), chosen such that little thickness variation occurred in the region used for cutting. To obtain mini-samples whose sides were perpendicular to their base, it was found necessary to ensure that the 2-mm cutter was kept precisely

perpendicular to the sheet during the cutting operation. This was accomplished by holding the square top of the 2-mm cutter securely against a press which pushes perpendicular to the sample sheet.

Compression stress relaxation (CSR) measurements were made using a Shawbury-Wallace Compression Stress Relaxometer MK II. This instrument uses special Shawbury-Wallace jigs (CSR jigs) to compress the cylindrical samples between adjustable metal platens. The standard sample was centered in the platens and then compressed to 25% strain at room temperature, after which initial force measurements were made. For the parallel mini-disk experiments, fifty mini-disk samples were spaced approximately uniformly and as close as possible to the center of the lower platen such that no contact would occur between adjacent mini-disks once they were compressed. Similar to the standard samples, approximately 25% average compression at room temperature was applied, followed by initial room temperature force measurements. The jigs were then placed in aging ovens for 1 day. After removal from the oven, they were allowed to equilibrate at room temperature before a sealing force measurement was made. The jigs were then returned to the oven for further aging. Periodically, additional force measurements were made using the same procedure.

Oxygen consumption rates were measured using a technique that has been described in detail elsewhere [21]. This technique monitors the change in oxygen content caused by reaction with polymer in sealed containers using gas chromatographic detection. Oven aging of the compression stress relaxation aging fixtures and the oxygen consumption containers was carried out in air-circulating ovens (±1°C) equipped with thermocouples connected to continuous strip chart recorders.

Oxygen permeation measurements were performed on an Oxtran-100 coulometric permeation apparatus (Modern Controls, Inc., Minneapolis, MN, USA), which is based on an ASTM Standard [22]. Several modifications, the most important of which was placing the sample holder in an oven, have been made to this instrument to permit data acquisition at higher temperatures (up to ~95°C for the present studies) with minimal temperature gradients (less than ±0.5°C) across the sample during the experiment.

Torsional relaxation experiments were run under flowing nitrogen gas on a Rheometrics RDS2 apparatus utilizing a parallel plate configuration on a 6.35 mm diameter, 1-mm thick disk. The rubber was placed in a room temperature vacuum chamber for 1 day prior to the run and then quickly transferred to the apparatus, where it was glued to copper platens using Loctite Quick Tite. At the beginning of the experiment, the sample was rapidly strained to 25% (ramp of less than 0.05 s), after which the stress was monitored versus time.

RESULTS AND DISCUSSION

For the compression stress-relaxation experiments at a given temperature, time-dependent values of Young's modulus $E(t)$ were obtained from rubber elasticity results as [23]

$$E(t) = \frac{3F(t)}{A\left(\lambda - \frac{1}{\lambda^2}\right)} \qquad (1)$$

where $F(t)$ is the force versus time measured at room temperature, A is the unstrained area of the disk sample and λ is the stretch ratio (1.25 for the current experiments). For the standard CSR experiments (disks of 12.7 mm initial diameter), conservation of volume during a 25% compression implies that the disks have diameters of approximately 14.7 mm during aging. CSR results at four temperatures ranging from 80°C to 125°C are plotted in Figs. 1 and 2. The decay in modulus with aging time observed in Figs. 1 and 2 typically results from a combination of physical and chemical effects [7-10]. Similar to the assumptions made by Curro and Salazar [7] and by Ito [9] in their attempts to separate these two components, we will assume that the overall modulus can be written as the product of the physical contribution in the absence of chemistry and the chemical part. Since chemical degradation for continuous stress-relaxation experiments is dominated by scission effects which lower the overall crosslink density ν, and the modulus is linearly related to ν, this assumption can be approximated as

$$E(t) = \frac{\nu(t)}{\nu_0} E_{phy}(t) \qquad (2)$$

where ν_0 is the initial crosslink density of the material and $E_{phy}(t)$ represents the physical relaxation. By obtaining estimates of the physical relaxation behavior at each temperature, eq. (2) will allow us to extract estimates of the chemical contribution.

Physical Relaxation Estimates

For a given temperature T, the following equation has been found to give a reasonable fit to physical stress-relaxation processes [7,24,25]

$$E_{phy}(t) = E_e\left[1 + \left(\frac{t}{\tau_T}\right)^{-m}\right] \qquad (3)$$

where, for a given material, E_e is the equilibrium modulus value, m is an empirical, temperature-independent constant and τ_T is a temperature-dependent time constant. This equation implies that a log-log plot of E_{phy} versus aging time t will give a curve whose instantaneous negative slope will decrease monotonically toward zero, a prediction consistent with countless experimental results. Our current objective is to obtain an estimate of this time-dependent slope for the aging times and temperatures used in this study. The earliest times accessed by the CSR experiments (Figs. 1 and 2) are after 1 day exposures, and the nature of the experiments preclude obtaining data at times shorter than several hours, since the thermal mass of the jigs requires an hour or so to establish thermal equilibrium when first placed in the oven. This means that, even at the lowest temperature of 80°C, significant chemical relaxation will occur over the several

days necessary to obtain an experimental estimate of the log-log slope. Thus it is impossible to use the CSR experiments to obtain estimates of the physical contributions. It is, however, easy to use related torsional relaxation experiments to probe the shorter time regions unavailable to the CSR approach. Figure 3 shows a log-log plot of 80°C and 100°C torsional relaxation data (25% strain) taken continuously from less than 1 second to ~ 1 hour. To minimize chemical relaxation effects, the experiments were run in a flowing nitrogen environment. As expected, the slopes of both curves decrease with aging time. In fact, the slope is already so low after 1 hour (absolute value <0.005), that after 1 day, physical relaxation can contribute at most a few percent to the relaxation observed in Figs. 1 and 2. We therefore ignore the physical contributions and conclude that the results shown in Figs. 1 and 2 are caused totally by chemical effects. Because E_{phy} is constant, eq. (2) implies

$$\frac{E(t)}{E(0)} \approx \frac{\nu(t)}{\nu_0} \tag{4}$$

where $E(0)$ is the time zero modulus value. As shown in Figs. 1 and 2, these values can be estimated by extrapolating the CSR data back to time zero.

Standard 15-mm CSR disks

We now examine the temperature dependence of the chemically dominated results from Figs. 1 and 2. If the semilog plots gave linear behavior at every temperature, we could extract the first-order rate constants from the slope, and we could plot the log of these rate constants versus inverse temperature to test the Arrhenius approach. Unfortunately, first-order behavior is not found at any of the temperatures. At 80°C and 95°C, linear behavior does occur after a more rapid drop at short times. At the higher temperatures of 110°C and 125°C, linear behavior may occur, but after a relatively longer, non-linear region. This change in relative shape of the degradation curves with temperature implies that the mechanism underlying the degradation is changing over this temperature range. This means that the Arrhenius model is not applicable since the underlying basis of the Arrhenius approach is that an increase in temperature accelerates all of the underlying chemical degradation mechanisms equally. This effect can be seen in Fig. 4, where we plot the log of the times to 50% and 75% loss in modulus versus inverse absolute temperature. The results for 50% loss in modulus give linear behavior, consistent with the Arrhenius assumption. However, the results for 75% loss in modulus show distinct non-Arrhenius behavior at the higher temperatures. For the Arrhenius expression to be valid, the same value of the activation energy E_a (slope) must hold regardless of the level of material damage.

Diffusion-limited oxidation (DLO) effects

The reason for the non-Arrhenius behavior found above is the presence of diffusion-limited oxidation effects, whose importance changes with aging temperature. For most polymeric materials, the presence of dissolved oxygen during aging causes oxidation chemistry to dominate the degradation. If the rate at which dissolved oxygen is used by reactions is faster

than the rate at which it can be replenished by diffusion from the surrounding air-atmosphere, a reduction in dissolved oxygen concentration will occur. This effect, which can lead to reductions in or elimination of oxidation in the interior regions of the material, is referred to as diffusion-limited oxidation [18,19,26]. To model this effect, diffusion expressions must be coupled with oxidative reaction rate expressions. A particularly useful and general kinetic rate expression is based on a variant of the basic autoxidation scheme (BAS), which has been utilized for more than 50 years [16,17] to describe the oxidation of organic materials. For stabilized materials, such as the present butyl elastomer, the simplified scheme can be written as follows [27]

Scheme 1. Classical oxidation scheme.

Initiation	$\text{Polymer} \xrightarrow{k_1} \text{R}\bullet$
Propagation	$\text{R}\bullet + \text{O}_2 \xrightarrow{k_2} \text{RO}_2\bullet$
Propagation	$\text{RO}_2\bullet + \text{RH} \xrightarrow{k_3} \text{RO}_2\text{H} + \text{R}\bullet$
Termination	$\text{RO}_2\bullet \xrightarrow{k_4=k_4'(\text{AH})} \text{Products}$
Termination	$\text{R}\bullet \xrightarrow{k_5=k_5'(\text{AH})} \text{Products}$
Branching	$\text{RO}_2\text{H} \xrightarrow{k_6} 2\text{R}\bullet + \text{ROH} + \text{HOH}$

Analysis of this scheme under steady state conditions for the two radical species and the ROOH concentration leads to the following expression for the oxygen consumption rate, ϕ:

$$\phi = \frac{d[\text{O}_2]}{dt} = \frac{C_1[\text{O}_2]}{1 + C_2[\text{O}_2]} \tag{5}$$

where

$$C_1 = \frac{k_1 k_2}{k_5} \tag{6}$$

$$C_2 = \frac{k_2(k_4 - 2k_3)}{k_5(k_3 + k_4)} \tag{7}$$

The result given by eq. (5) has been shown to be in excellent agreement with experimental results for several stabilized elastomers, including a nitrile rubber and a neoprene rubber [19].

Equation (5), the expression for the oxygen consumption rate, has been combined with standard diffusion expressions [28] to model diffusion-limited oxidation (DLO) effects for samples with planar geometry [15]. The resulting theoretical expressions have been shown to give quantitative agreement with experimental results for both thermoxidative [19] and radiation-oxidative aging [18,20] of elastomers. Since we are unaware of any work on analogous DLO modeling of disk-shaped samples using the oxidation expression shown in eq. (5), we have applied finite element methods to obtain solutions to this problem. The CSR sample was modeled as a cylindrical disk having unit thickness and radius *a*. The axis symmetric geometry used is shown in Fig. 5.

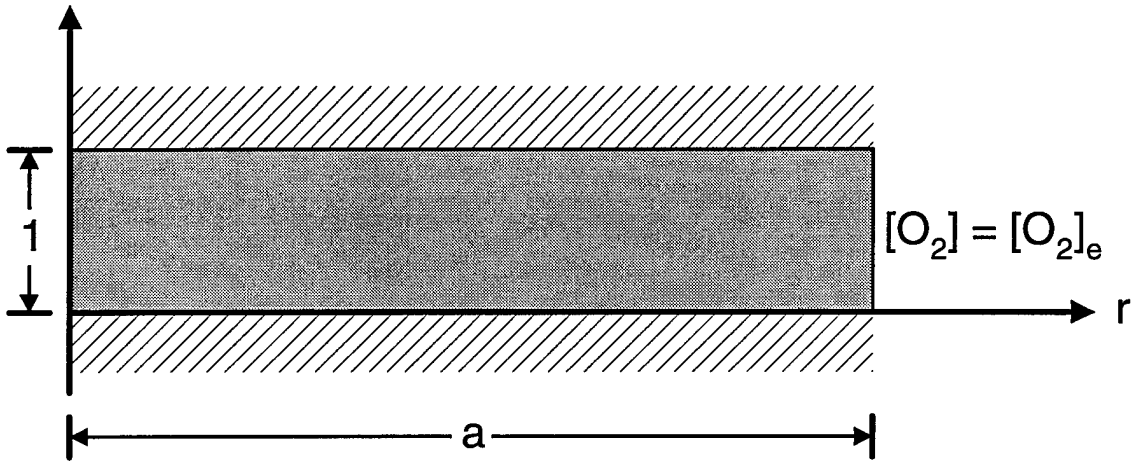

Fig. 5. The axis symmetric geometry used for the modeling of the CSR experiment.

For the modeling, the oxygen concentration is given by $[O_2]$ and the planar surfaces of the disk are taken to be impermeable. In this case, diffusion is one-dimensional and the appropriate diffusion-reaction equation in the radial coordinate is [28]:

$$\frac{1}{r}\frac{\partial}{\partial r}\left(rD\frac{\partial[O_2]}{\partial r}\right)=\frac{C_1[O_2]}{1+C_2[O_2]} \tag{8}$$

with boundary conditions: $[O_2] = [O_2]_e$ at r = a. *D* is the diffusion coefficient, which is assumed to be constant, and C_1 and C_2 are the reaction rate constants given in eqs. (6) and (7). The equation may be put in dimensionless form by making the substitutions: R = r/a, and $\theta = [O_2]/[O_2]_e$. Hence, the dimensionless diffusion-reaction equation becomes:

$$\frac{1}{R}\frac{\partial}{\partial R}\left(R\frac{\partial\theta}{\partial R}\right)=\frac{\alpha'\theta}{1+\beta\theta} \tag{9}$$

with $\theta = 1$ at R = 1. The parameters α' and β are given by

$$\alpha' = \frac{C_1 a^2}{D} \tag{10}$$

$$\beta = C_2 Sp = C_2 [O_2]_e \tag{11}$$

where p is the oxygen partial pressure surrounding the sample and S is the oxygen solubility coefficient for the polymer (the permeability coefficient, P_{Ox} is the product of D and S). The parameter α' is used here to distinguish the disk theory from the theory for sheet material which utilizes the parameter α [15]. It is clear from eqs. (10) and (11) that β can be changed by changing the oxygen partial pressure surrounding the sample and that α' is a geometry-sensitive parameter that can be changed by changing the sample diameter.

The finite element method with Newton-Raphson iteration [29] was used to solve the non-linear, dimensionless diffusion-reaction equation on a mesh consisting of 100 intervals in the radial coordinate. The disk was initially devoid of oxygen and the iteration proceeded until the steady-state oxygen profile was achieved. Using this procedure, normalized, steady-state oxygen concentration profiles were obtained as a function of radial position for various combinations of the parameters α' and β. From the oxygen concentration profiles, oxidation rate profiles relative to the surface oxidation rates were obtained by using the relationship:

$$\text{Relative Oxidation} = \frac{\alpha' \theta(R)}{1 + \beta \theta(R)} \Big/ \frac{\alpha'}{1+\beta} \tag{12}$$

where use has been made of the fact that $\theta(1) = 1$. Some typical relative oxidation profiles are shown in Fig. 6 for $\beta = 1$; this value of β is a typical result for elastomers aged in air [19].

By multiplying both sides of eq. (5) by a^2/pP_{Ox}, the following useful relationship is obtained for disk-shaped samples

$$\frac{\phi a^2}{pP_{Ox}} = \frac{\alpha'}{1+\beta} \qquad \text{(disk-shaped case)} \tag{13}$$

This expression is almost identical to the result obtained for sheet material of thickness L, given by

$$\frac{\phi L^2}{pP_{Ox}} = \frac{\alpha}{1+\beta} \qquad \text{(sheet case)} \tag{14}$$

In several recent studies of planar samples [18-20], we have shown that experimental oxidation profiles for elastomers aged in both radiation and thermoxidative environments are quantitatively consistent with both the profile shapes predicted by the theory and with eq. (14).

This implies that we can confidently use our modeling to estimate the experimental conditions where diffusion-limited oxidation effects are important. We do this by first integrating the relative theoretical oxidation results across the samples (this gives the amount of oxidation relative to a homogeneously oxidized material) and then deciding at what percentage level diffusion effects become unimportant. For planar results, the integration procedure is straightforward. For the disk-shaped samples, the integrated relative oxidation (IRO) in percent can be computed from the relative oxidation profiles by integrating the profiles over the volume of the disk in the cylindrical coordinate system:

$$\text{Integrated Relative Oxidation (\%)} = 100\int_0^1 \left[\frac{\alpha'\theta(R)}{1+\beta\theta(R)} \Big/ \frac{\alpha'}{1+\beta}\right] R dR \Big/ \int_0^1 R dR \qquad (15)$$

In the present case, the integral in the numerator was evaluated by numerical integration of the oxidation profile using the trapezoidal rule. Results for IRO plotted versus values of α' and β are shown in Fig. 7.

To use the theoretical results for estimates of the importance of DLO for our samples, we need estimates versus temperature of the oxygen consumption rate and the oxygen permeability coefficient. Figure 8 plots oxygen consumption results versus aging time at 95°C and 110°C. At 110°C, the consumption rate drops by approximately a factor of 2 over the first 20 to 30 days an then remains relatively constant. The limited data at 95°C show indications of similar behavior at early times. The results from these two temperatures can be integrated to give oxygen consumption results versus time and then time-temperature superposed [1,21,27]. The time-temperature superposition approach involves empirically shifting the time scale for the data at a temperature T by multiplying the times by a constant shift factor a_T such that the time-shifted results give the best overlap (superposition) with data at a selected reference temperature ($a_T = 1$ at the reference temperature). The principle underlying this approach is that degradation curves at two temperatures must have time scales that are related by a constant multiplicative factor if raising the temperature results in a constant acceleration of the underlying degradation chemistry. Although we have very limited oxygen consumption data for this material, extensive previous work on oxygen consumption results indicates that such data give excellent time-temperature superposition [19,21,27]. If we select 95°C as the reference temperature, the best superposition of the 110°C data occurs when we multiply the times associated with this data by a factor of 3.2. Figure 9 shows the resulting superposed data.

An acceleration factor of 3.2 between 95°C and 110°C corresponds to an Arrhenius activation energy of ~91 kJ/mol. From Fig. 1, we note that substantial force decay occurs for the 15-mm disk at 95°C over approximately 150 days. Using the shifted results from Fig. 9, we can estimate that the average oxygen consumption rate ϕ_{ave} over ~150 days at 95°C is ~2.8e-11 mol/g/s. Since an acceleration factor of 3.2 times occurs when T increases from 95°C to 110°C, we estimate that ϕ_{ave} at 110°C is equal to 9e-11 mol/g/s. To obtain ϕ_{ave} estimates at the other two temperatures of interest, 80°C and 125°C, we assume Arrhenius behavior with an activation energy of 91 kJ/mol, as derived above. Table I summarizes the estimates for ϕ_{ave}. Measurements of the other required parameter, P_{Ox}, were made at four temperatures ranging

from ~30°C to 95°C. The results, which are shown in Fig. 10, allow estimates to be made for P_{Ox} at the four temperatures of interest; these estimates are also given in Table I.

Table I. Estimates of the importance of DLO effects for CSR samples.

Conditions	T, °C	125	110	95	80
	ϕ_{ave}, mol/g/s	2.6e-10	9e-11	2.8e-11	8e-12
	P_{Ox}, ccSTP/cm/s/cmHg	5.55e-9	3.75e-9	2.3e-9	1.25e-9
β=3, a=7.33mm	α'/IRO	200/31%	100/43%	51/57%	27/73%
β=1, a=7.33mm	α'/IRO	100/29%	50/40%	26/53%	13.4/67%
β=0.3, a=7.33mm	α'/IRO	65/27%	33/37%	17/49%	8.6/63%
β=1, a=1.15mm	α'/IRO	2.5/92%	1.25/96%	0.64/98%	0.33/99%

With the above estimates of ϕ_{ave} and P_{Ox} versus temperature, we can now use eq. (13) to estimate the importance of DLO for the 15-mm standard size CSR disks. Given that the partial pressure of oxygen in Albuquerque is 13.2 cmHg and the density of the butyl material is 1.15 g/cc, eq. (13) can be rewritten as

$$\alpha' = \frac{\phi\, a^2(\beta+1)}{P_{Ox}} \frac{(2.24e4 ccSTP/mol)(1.15 g/cc)}{(13.2 cmHg)} \tag{16}$$

Since we have estimates of ϕ_{ave} and P_{Ox} versus temperature (Table I) and we know that a is 7.33 mm for our standard CSR disks, we can use eq. (16) to calculate values of α' if values of β are known. It turns out, however, that the results are relatively insensitive to the values of β , as will be seen shortly. For thermoxidative aging of elastomers in air environments, β is typically found to be close to unity [19], so we will assume a similar situation for the butyl material. We therefore use values of β equal to 3, 1 and 0.3 to obtain values of α' as a function of temperature; the results are summarized in rows 4 to 6 in Table I, together with the corresponding IRO values determined from Fig. 7. These results show the relative insensitivity of IRO to β , but also indicate that substantial DLO effects are present for the 15-mm CSR disk samples. At 80°C, the integrated oxidation is ~67% of a homogeneously oxidized material; at 125°C, the oxidation drops to ~29%. These estimates are noted on the Arrhenius plot (Fig. 4). It is now clear that the non-Arrhenius behavior and the low activation energy observed for these results are due to DLO effects which are becoming more important as the temperature is increased.

Parallel mini-disk approach

To minimize the DLO anomalies noted for the standard 15-mm samples, fifty 2-mm disk samples were carefully prepared and strained in parallel as noted in the Experimental section. Experiments were run at 125°C, 110°C and 95°C (long-term runs at 80°C and 70°C are

currently underway). When the strained value of a appropriate to these experiments (1.15 mm) is used in eq. (16) together with a β value of unity, the modeling leads to the IRO values listed in the last row of Table I. These results imply that the amount of oxidation for the minidisk samples will range from ~92% at 125°C to 98% at 95°C, essentially eliminating concerns over important DLO effects. Results for the log of the relative force (force divided by the extrapolated, time-zero force) versus linear time are plotted for 95°C and 110°C data in Fig. 11 and for 125°C data in Fig. 12 (open squares). Except for a slightly faster drop at early times, the data at all temperatures follow approximately first-order decay for the bulk of the degradation process. First-order behavior is consistent with a constant rate of scission, as noted in eq. (4). It is interesting to compare the 15-mm and 2-mm normalized results at a given temperature. Such a comparison is shown for the 125°C data in Fig. 12; as expected, the force decay of the 15-mm sample, which is influenced by significant DLO effects, is much slower than the true decay obtained in the absence of important diffusion anomalies.

If we carry out an analysis of the 2-mm results similar to that done on the 15-mm samples in Fig. 4 by plotting the log of the times to 50% and 75% loss of force versus inverse absolute temperature, we obtain the results shown in Fig. 13. In this case, we obtain linear behavior with similar slopes for both levels of damage. These results are therefore consistent both with the Arrhenius relationship predicting that the change in degradation rate is proportional to the exponential of the inverse temperature and with the constant acceleration assumption underlying the Arrhenius approach. In addition, the activation energy of ~84 kJ/mol (20 kcal/mol) derived from the slope is consistent with the range of values normally found for oxidative degradation of elastomers (80-120 kJ/mol). If we assume that no change in activation energy occurs at temperatures lower than 95°C, we can extrapolate the results to lower temperatures to make lifetime predictions.

Since the results in Fig. 13 offer strong evidence that constant acceleration occurs for changes in aging temperature, the time-temperature superposition approach offers a better method for analyzing these data. We apply this technique by first selecting 95°C as the reference temperature ($a_T = 1$). We then adjust the time scales for degradation at the other temperatures by finding the empirical multiplicative factor, a_T which, when multiplied times the experimental times, gives the best overlap of the higher temperature results with the reference results. For the current results, excellent superposition occurs when the 110°C time scale is multiplied times 3.2 and the 125°C time scale is multiplied by 8, as shown in Fig. 14. The most important advantage of the time-temperature superposition approach compared to the procedure used in Fig. 13, is that the former utilizes all of the experimental data, not a truncated and processed set. Not surprisingly, when the log of the empirically derived shift factors ($a_T = 1$, 3.2 and 8) are plotted versus inverse absolute temperature, approximately linear behavior results, yielding an Arrhenius activation energy close to that found in Fig. 13. The superposed results of Fig. 14 again show the faster early drop in the relative force, followed by a linear, first-order like decay. The dashed line through the bulk of the data can be used to estimate that the first-order rate constant for this part of the data is 0.0113/d. The dashed line through the early data is a crude attempt to estimate the initial rate constant at 95°C (~0.021/d), a value approximately twice as large as the longer term rate constant.

It is interesting to note that the empirically derived oxygen consumption shift factor at 110°C relative to a 95°C reference temperature (Fig. 9) is exactly identical to that found for the force decay in Fig. 14 ($a_T = 3.2$). This offers strong evidence that the oxidation chemistry is intimately connected to the force decay, which is not surprising since scission is often caused by oxidative processes. This connection is even more apparent when we replot the superposed data of Fig. 9 on a linear-linear plot. The results, which are shown in Fig. 15, imply that the early time oxygen consumption rate (from the slope of the data) is approximately two times the later-time results, similar to the ratio found in Fig. 14 for the force decay data. Comparing Figs. 14 and 15, therefore, strongly suggests that the force decay is caused by oxidative scission processes, and the reason for the faster force drop in the initial stages is a correspondingly larger oxidation rate in the early stages of degradation. This apparent correlation implies that it may be possible to predict how the slope of the Arrhenius curve behaves at temperatures much lower than 70°C by measuring oxygen consumption rates at low temperatures, similar to the procedures we have used previously for quantitatively testing the Arrhenius extrapolation assumption [21,27].

CONCLUSIONS

We have determined that CSR experiments on standard 15 mm disks of a butyl material lead to complex non-Arrhenius behaviors. Through the use of theoretical diffusion-limited oxidation (DLO) modeling for disk-shaped geometry, we offered evidence that important DLO effects were the cause of the non-Arrhenius behavior and that 2 mm disks are required to eliminate DLO effects for this butyl material. By carrying out CSR experiments on fifty 2 mm disk samples strained in parallel, Arrhenius behavior with an activation energy of 84 kJ/mol was obtained. Assuming this E_a remains constant, the Arrhenius results can be extrapolated to make predictions at temperatures lower than the temperature range (125°C to 95°C) used for the CSR experiments. We are currently collecting long-term CSR data at 80°C and 70°C to see if the E_a remains constant from 95°C down to 70°C. In addition, we observed a correlation between the CSR force decay and the oxygen consumption rate, suggesting that oxygen consumption measurements below 70°C may allow us to confirm extrapolations below this temperature. Detailed oxygen consumption measurements at various temperatures down to 23°C are currently underway.

ACKNOWLEDGMENTS

Sandia is a multiprogram laboratory operated by Sandia Corporation, a Lockheed Martin Company, for the United States Department of Energy under Contract DE-AC04-94AL85000. The authors gratefully acknowledge Doug Adolf for carrying out the shear relaxation experiments and Mike Malone, who conducted the CSR experiments.

REFERENCES

1. J. D. Ferry, Viscoelastic Properties of Polymers, 2nd Ed., Wiley, New York, 1970.
2. A. V. Tobolsky, Properties and Structure of Polymers, Wiley, New York, 1960.

3. K. Murakami and K. Ono, Chemorheology of Polymers, Elsevier Publishing Co., Amsterdam, 1979.
4. K. P. Fernando, A. W. Birley and C. Hepburn, Polymer Testing, 5, 209 (1983).
5. J. C. Armah, A. W. Birley, K. Fernando, C. Hepburn and M. Tahir, Rubber Chem. Tech., 59, 765 (1983).
6. A. W. Birley, K. P. Fernando and M. Tahir, Polymer Testing, 6, 85 (1986).
7. J. G. Curro and E. A. Salazar, J. Appl. Polym. Sci., 19, 2571 (1975).
8. B. Stenberg and J. F. Jansson, Rubber Chem. Tech., 50, 906 (1977).
9. M. Ito, Polymer 23, 1515 (1982).
10. K. Murakami, S. Tamura and H. Oikawa, in H. H. G. Jellinek (ed.) Degradation and Stabilization of Polymers, Elsevier, Amsterdam, 1983.
11. K. Ono, A. Kaeriyama and K. Murakami, J. Polym. Sci., P. C. Ed., 13, 2615 (1975).
12. K. Ono, A. Kaeriyama and K. Murakami, J. Polym. Sci., P. C. Ed., 16, 1575 (1978).
13. K. Murakami, K. Ono and H. Oikawa, Polym. Engin. Rev., 3, 197 (1983).
14. Reference 10, page 495.
15. A. V. Cunliffe and A. Davis, Polym. Degradation Stab., 4, 17 (1982).
16. J. L. Bolland, Proc. R. Soc. London, A186, 218 (1946).
17. L. Bateman, Q. Rev. (London), 8, 147 (1954).
18. K. T. Gillen and R. L. Clough, Polymer, 33, 4358 (1992).
19. J. Wise, K. T. Gillen and R. L. Clough, Polymer, 38, 1929 (1997).
20. J. Wise, K. T. Gillen and R. L. Clough, Radiat. Phys. and Chem., 49, 565 (1997).
21. J. Wise, K. T. Gillen and R. L. Clough, Polym. Degrad. & Stabil., 49, 403 (1995).
22. ASTM Standard D3985-81- Oxygen Gas Transmission Rate through Plastic Film and Sheeting Using a Coulometric Sensor.
23. L. G. Treloar, The Physics of Rubber Elasticity, Oxford University Press, London, 1958.
24. R. Chasset and P. Thirion in Proc. Int. Conf. Noncrystalline Solids, North-Holland, Amsterdam, 1965.
25. D. Plazek, J. Polym. Sci., A2, 811 (1964).
26. K. T. Gillen and R. L. Clough, in Handbook of Polymer Science and Technology, Vol. 2, N. P. Cheremisinoff, Ed., Marcel Dekker, New York, 1989, Ch. 6.
27. K. T. Gillen, M. Celina, R. L. Clough and J. Wise, Trends in Polymer Science, Vol 5, No. 8, 250 (August, 1997).
28. J. Crank, The Mathematics of Diffusion, Clarendon Press, Oxford, 1975.
29. K. H. Huebner and E. A. Thornton, Finite Element Method for Engineers, 2nd Ed., Wiley, New York, 1982.

FIGURE CAPTIONS

Fig. 1. Time-dependent compression stress relaxation modulus for standard disk samples at 80°C and 95°C.

Fig. 2. Time-dependent compression stress relaxation modulus for standard disk samples at 110°C and 125°C.

Fig. 3. Time-dependent torsional relaxation data in nitrogen at 80°C and 100°C.

Fig. 4. Arrhenius plot of the log of the times required to reduce the CSR modulus by 50% and 75% versus the inverse absolute aging temperature using data from Figs. 1 and 2. Percentage shown at each temperature gives theoretical estimate of sample oxidation relative to a homogeneously oxidized material.

Fig. 5. The axis symmetric geometry used for modeling of the CSR experiments.

Fig. 6. Representative relative oxidation profiles for $\beta = 1$ (a typical value for elastomers in air) and various values of α'.

Fig. 7. Plot of selected Integrated Relative Oxidation values (in percentage oxidized) versus α' and β.

Fig. 8. Oxygen consumption rates for the butyl material as functions of aging time at the indicated temperatures.

Fig. 9. Empirical time-temperature superposition of the integrated form of the data from Fig. 8 at a reference temperature of 95°C. The values of a_T used are indicated.

Fig. 10. Oxygen permeability coefficient measurements for the butyl material plotted versus inverse absolute temperature.

Fig. 11. Time-dependent compression stress relaxation force data (normalized to zero time) for 50 parallel-strained 2 mm diameter disks at 95°C and 110°C.

Fig. 12. Comparison of the time-dependent compression stress relaxation force data (normalized to zero time) for 50 parallel-strained 2 mm diameter disks and a standard 15 mm disk sample at 125°C.

Fig. 13. Arrhenius plot for the parallel mini-disk CSR experiments. The log of the times required for the normalized force results to drop by 50% and 75% are plotted versus the inverse absolute aging temperature using data from Figs. 11 and 12. Percentage shown at each temperature gives theoretical estimate of sample oxidation relative to a homogeneously oxidized material.

Fig. 14. Empirical time-temperature superposition of the normalized force data for the parallel mini-disk results shown in Figs. 11 and 12. The values of a_T used are indicated.

Fig. 15. Empirical time-temperature superposed oxygen consumption data of Fig. 9 replotted on a linear-linear scale.

(1)

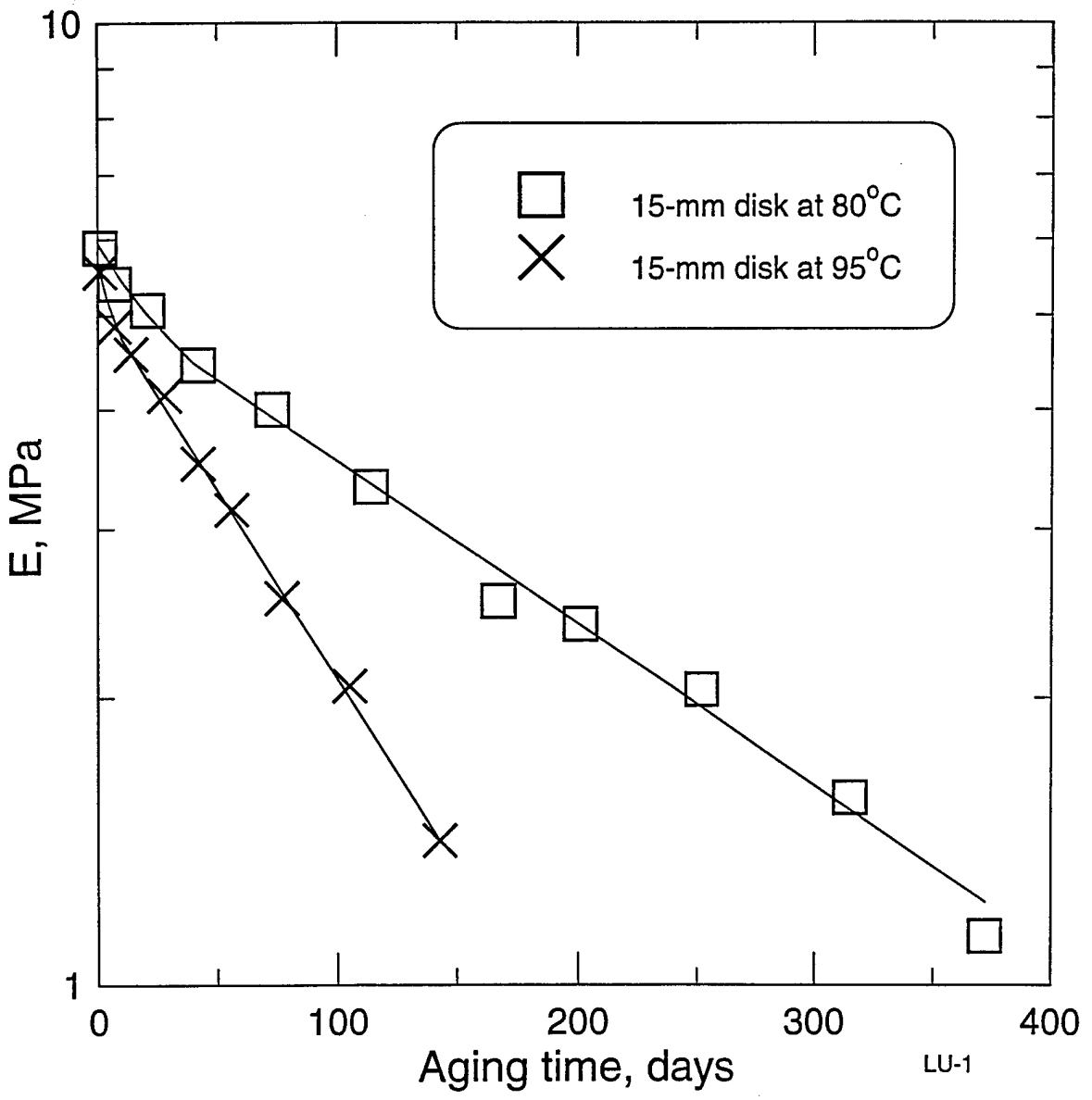
10
1
E, MPa
0
100
200
300
400
Aging time, days
15-mm disk at 80°C
15-mm disk at 95°C
LU-1

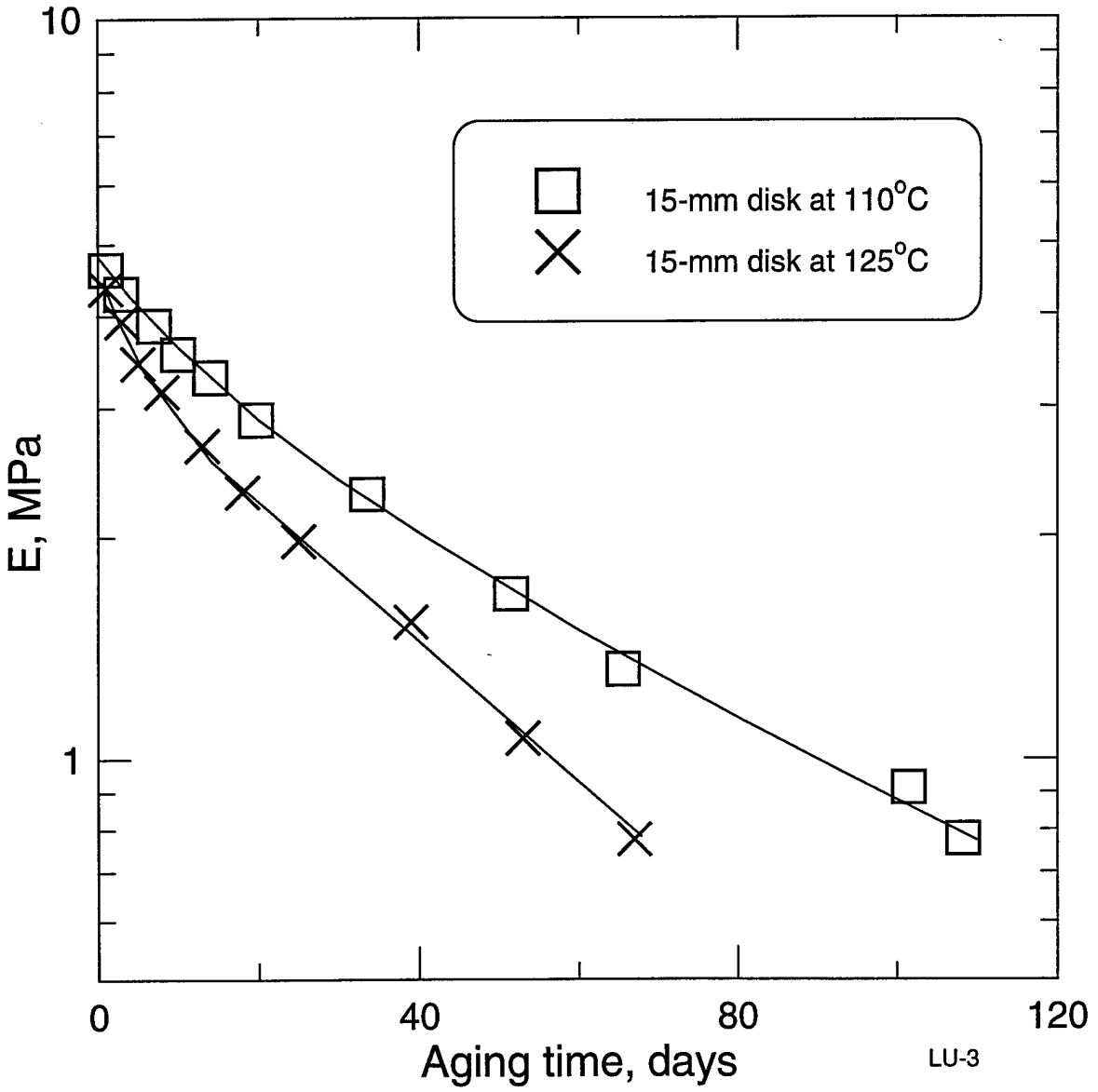
10
1
E, MPa
0
40
80
120
Aging time, days
15-mm disk at 110°C
15-mm disk at 125°C
LU-3

3

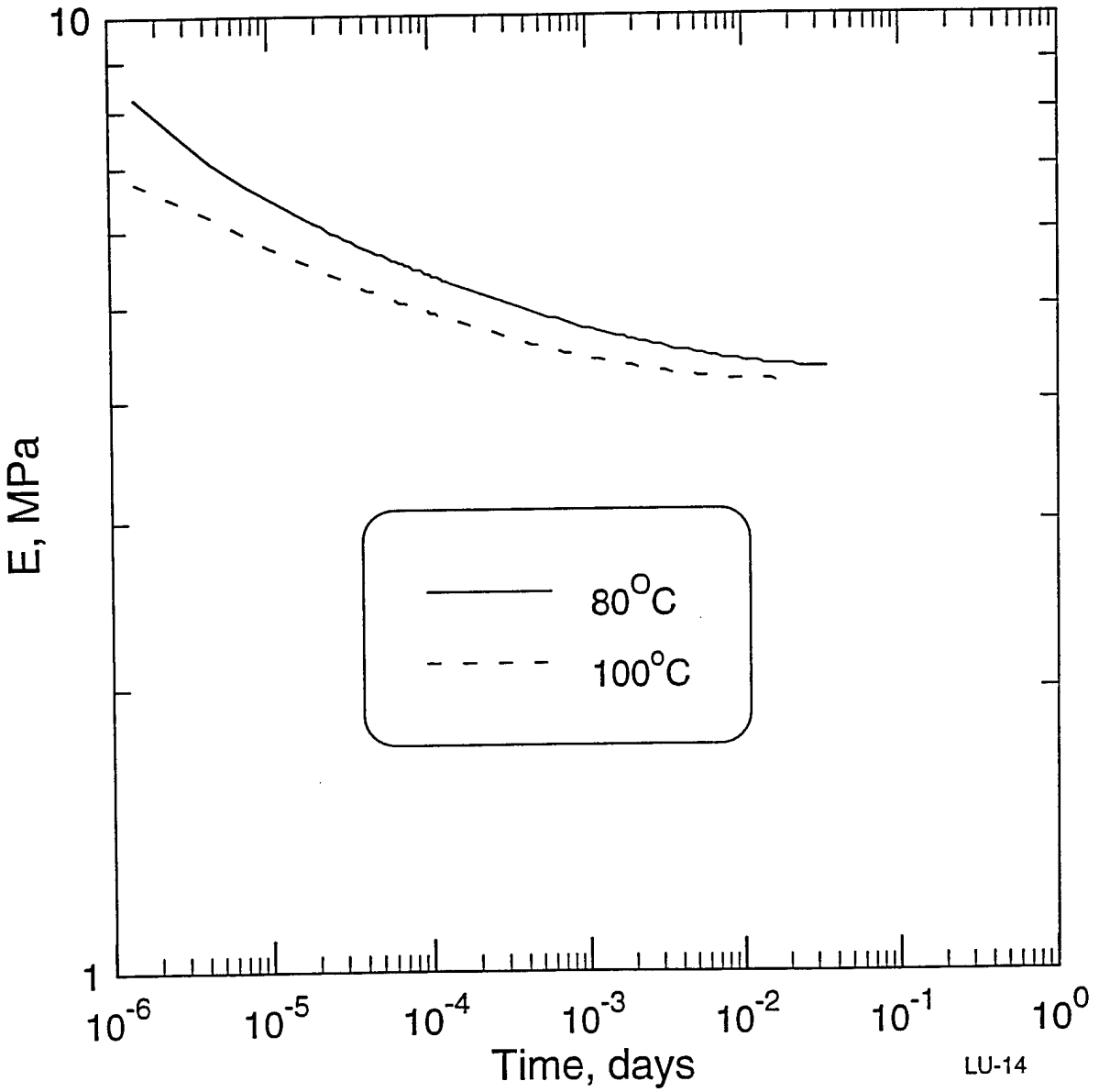

(4)

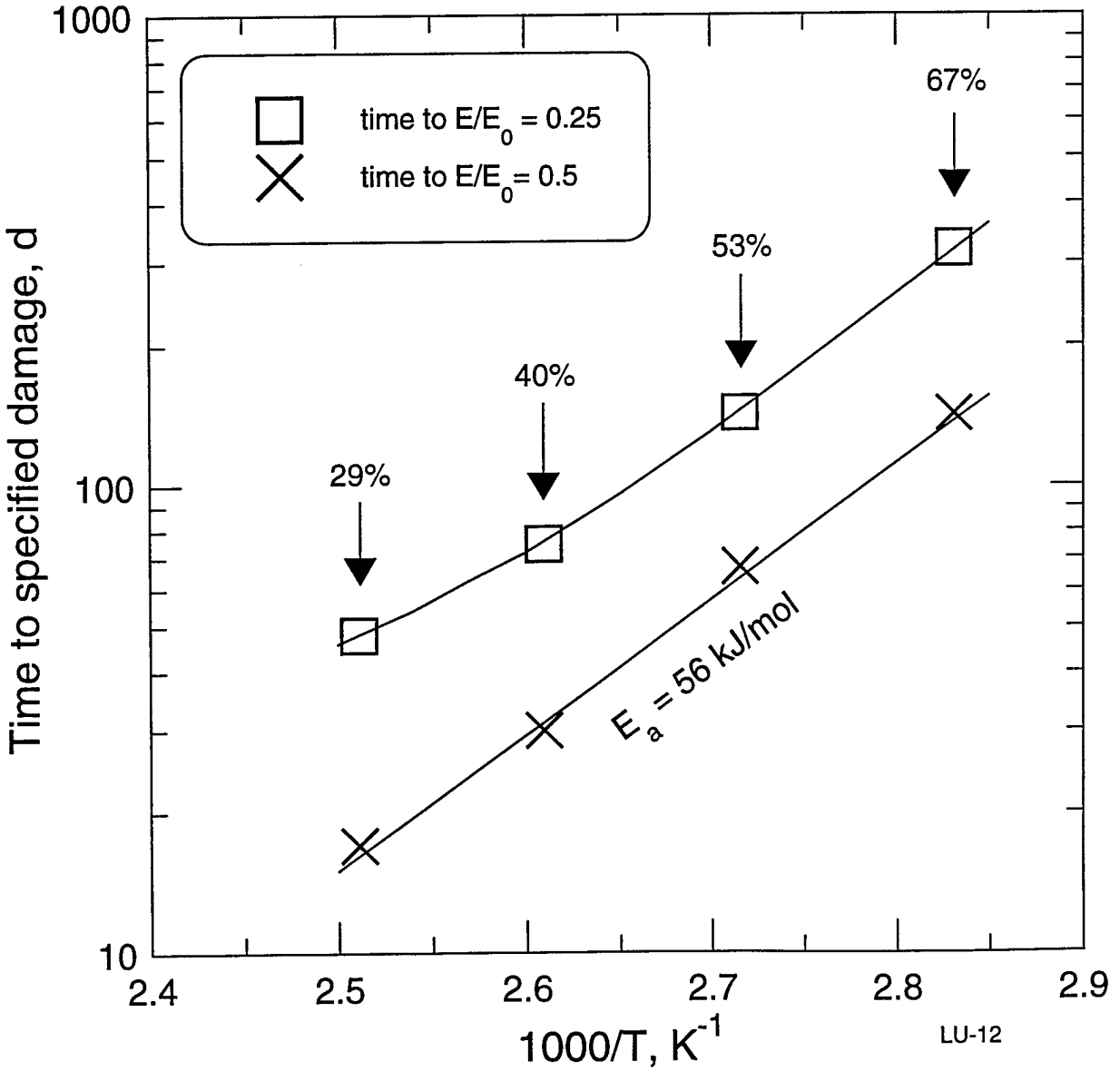
1000
100
10
Time to specified damage, d
time to E/E0 = 0.25
time to E/E0 = 0.5
67%
53%
40%
29%
Ea = 56 kJ/mol
2.4
2.5
2.6
2.7
2.8
2.9
1000/T, K-1
LU-12

(5)

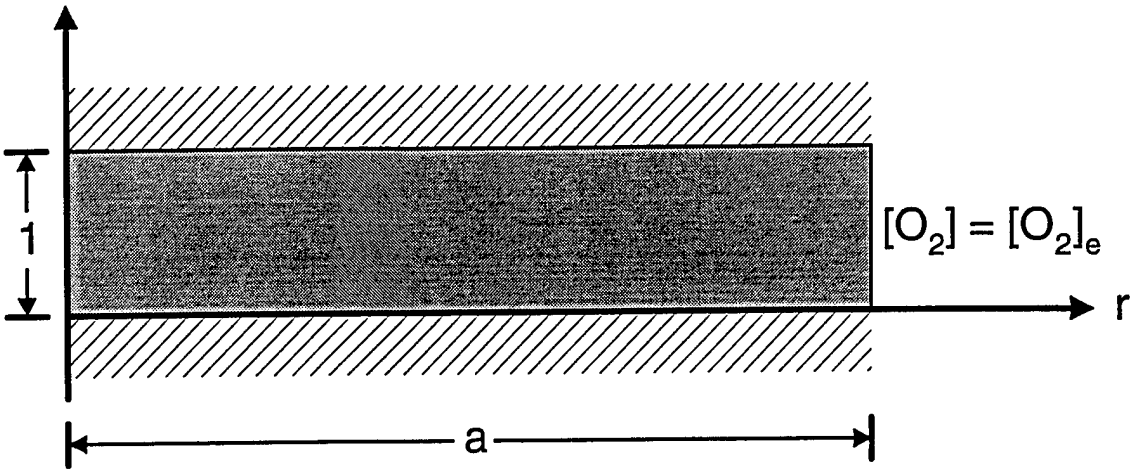

6

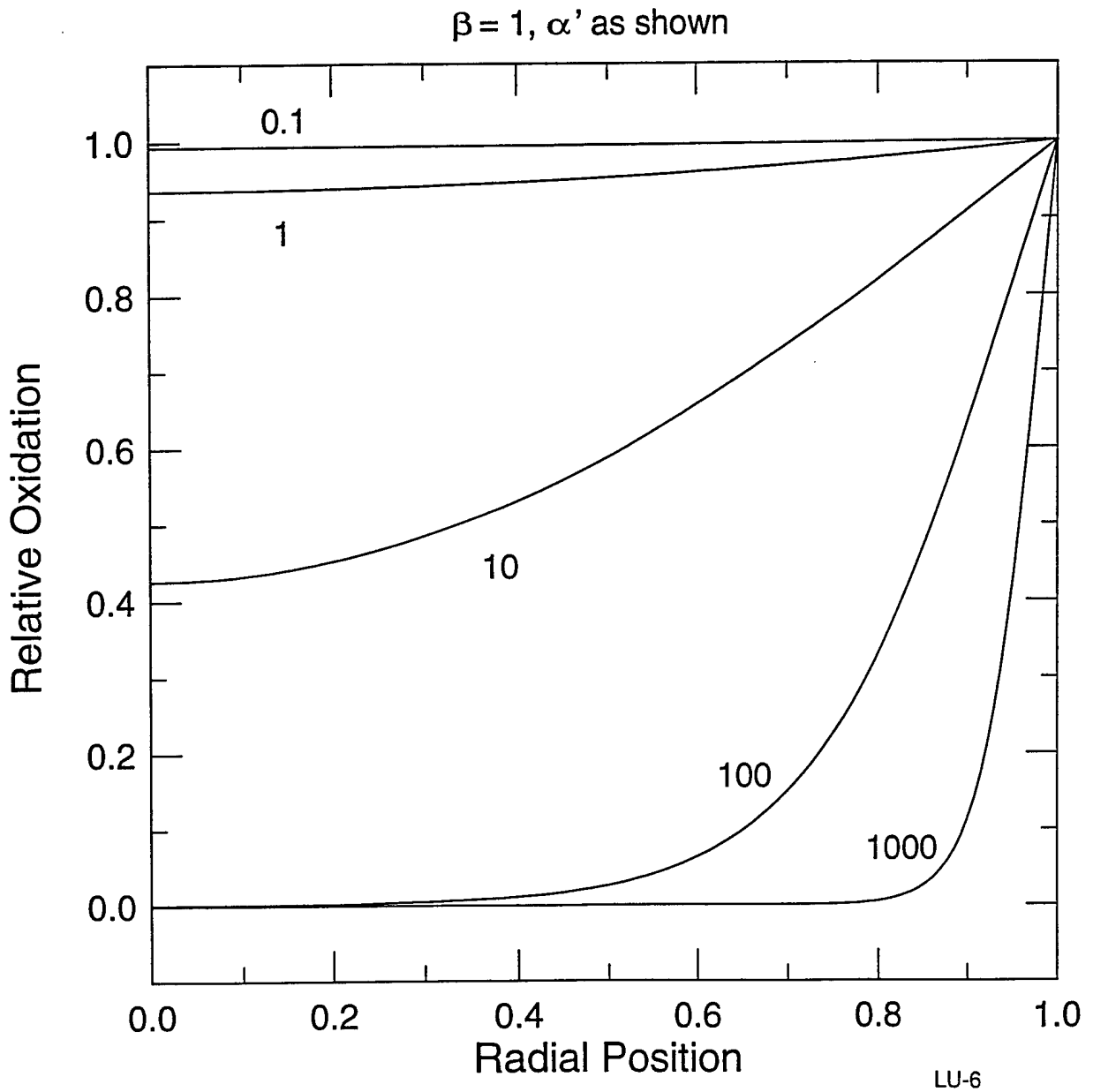
β = 1, α' as shown
0.1
1
10
100
1000
1.0
0.8
0.6
0.4
0.2
0.0
Relative Oxidation
0.0
0.2
0.4
0.6
0.8
1.0
Radial Position
LU-6

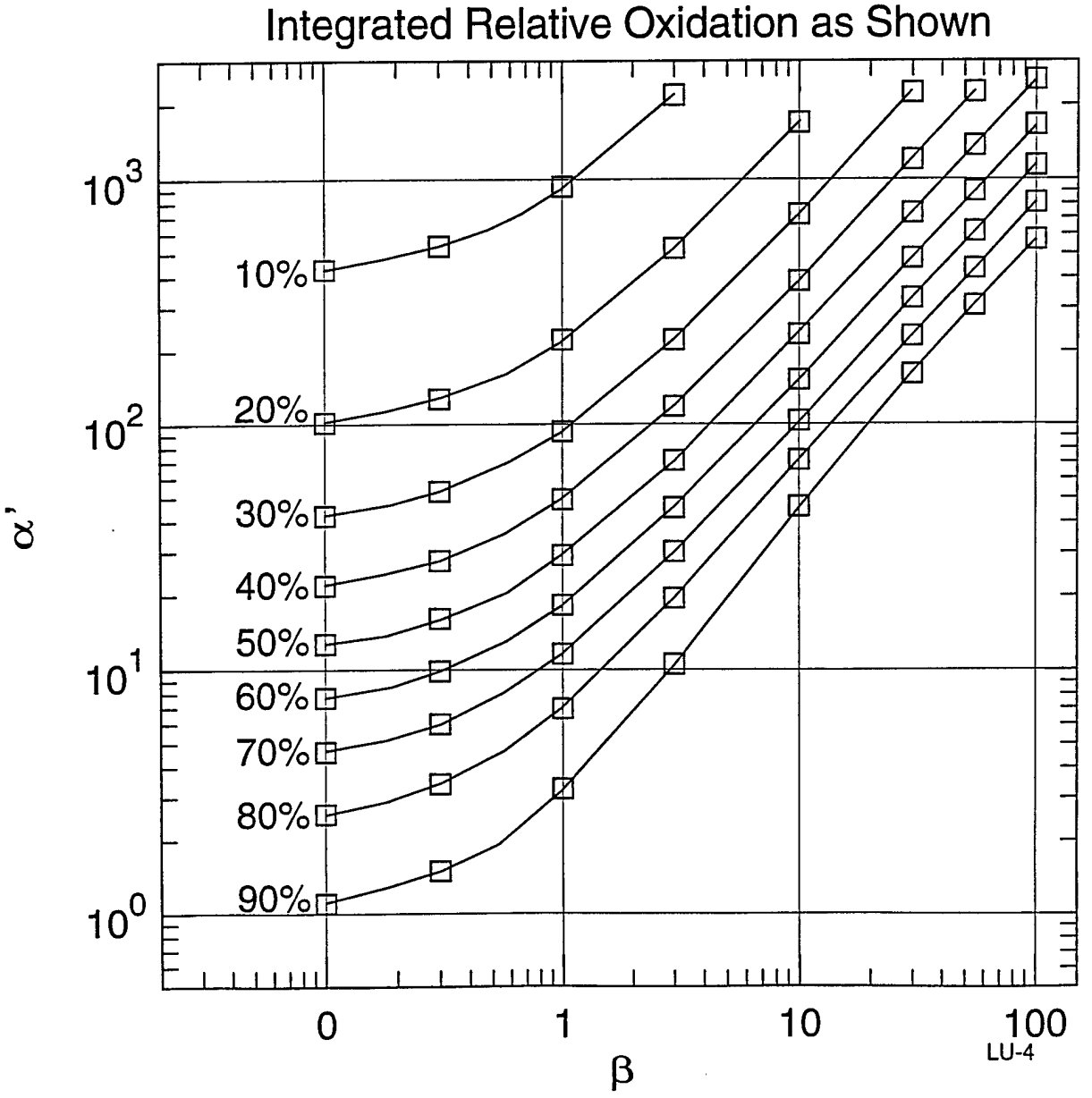
Integrated Relative Oxidation as Shown
10^3
10^2
10^1
10^0
α'
10%
20%
30%
40%
50%
60%
70%
80%
90%
0
1
10
100
β
LU-4

(8)

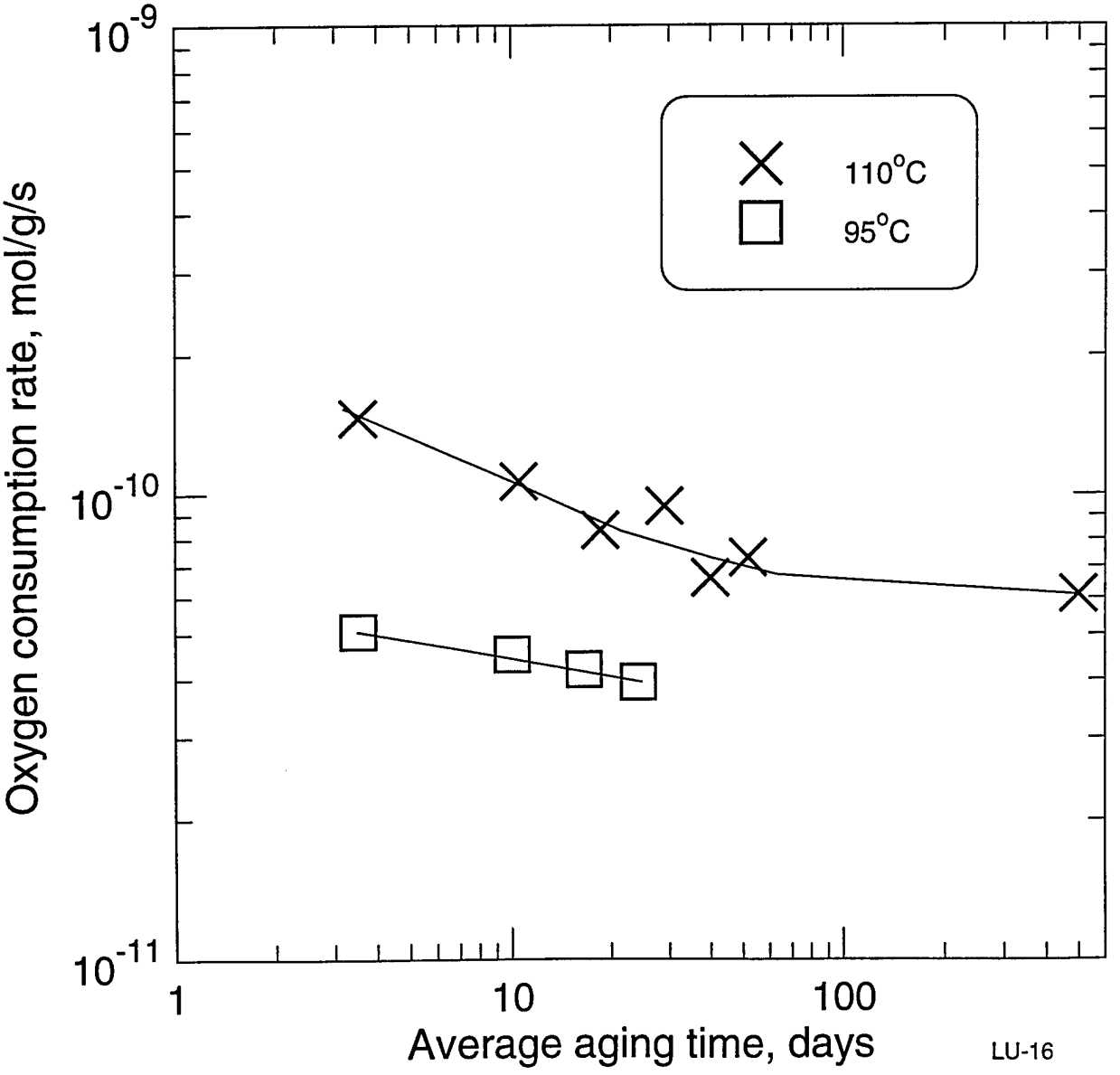
10^{-9}
10^{-10}
10^{-11}
Oxygen consumption rate, mol/g/s
110°C
95°C
1
10
100
Average aging time, days
LU-16

9

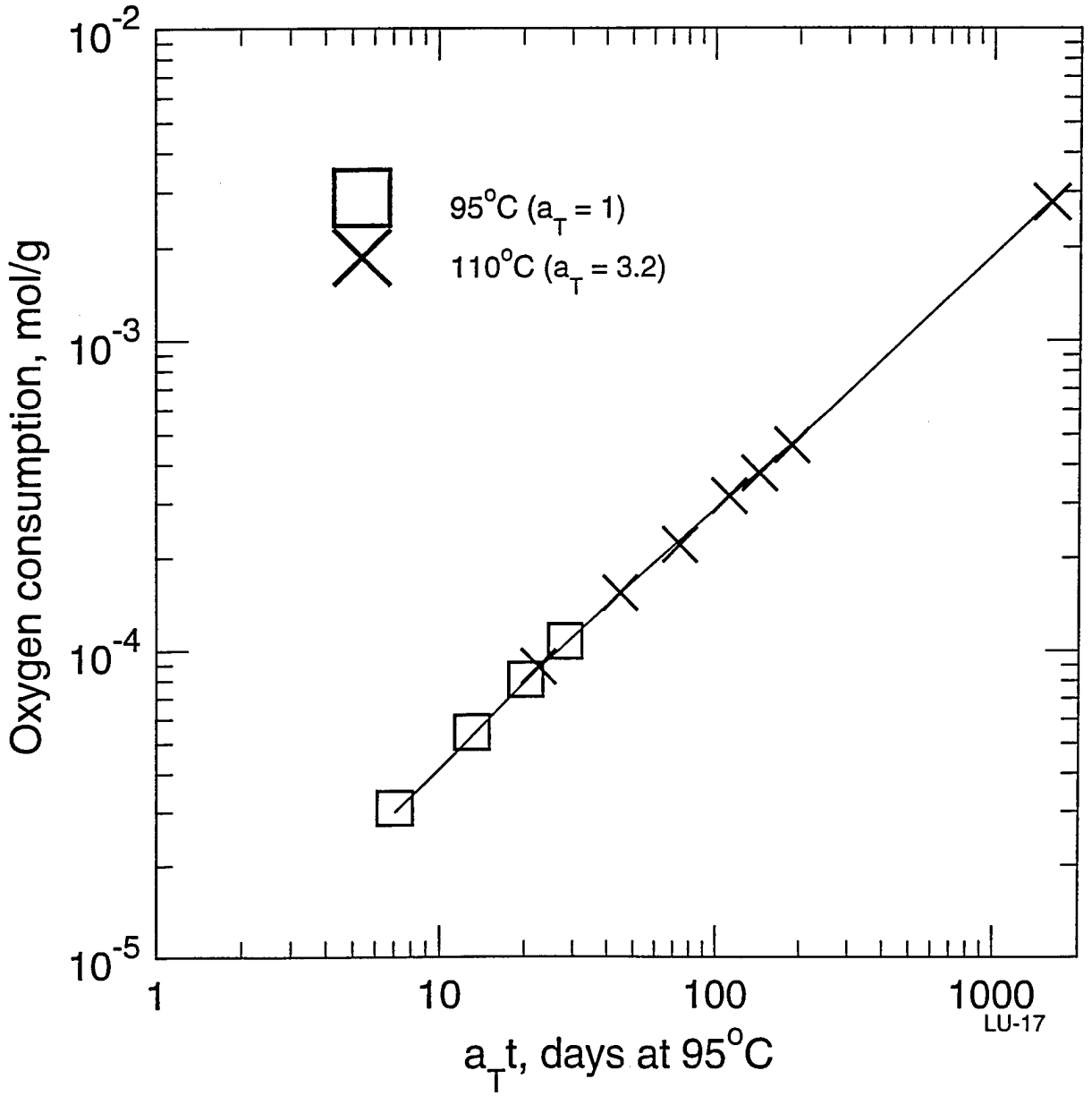
10^{-2}
10^{-3}
10^{-4}
10^{-5}
Oxygen consumption, mol/g
95°C (a_T = 1)
110°C (a_T = 3.2)
1
10
100
1000
a_Tt, days at 95°C
LU-17

(10)

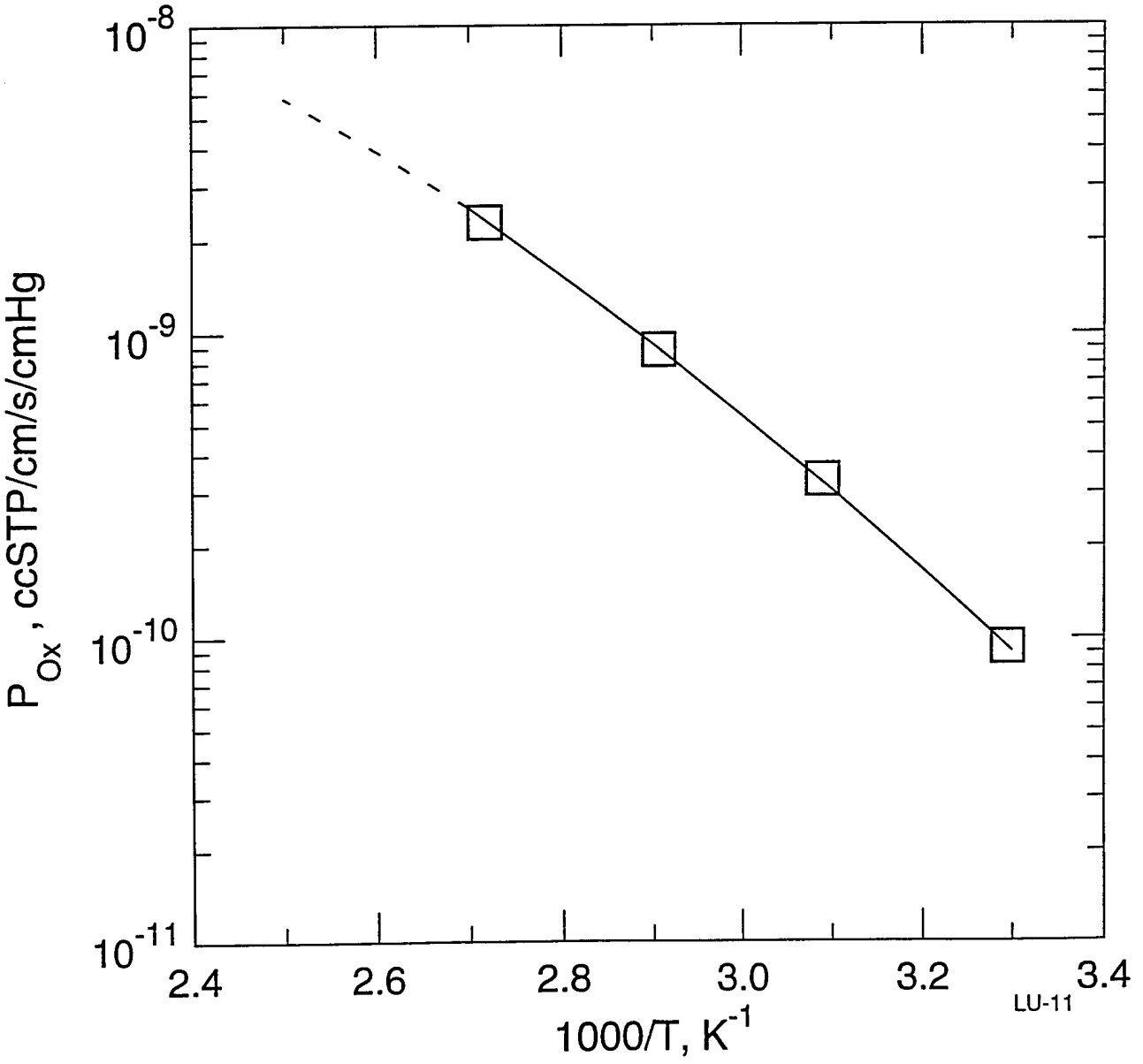
10^{-8}
10^{-9}
10^{-10}
10^{-11}
P_{Ox}, ccSTP/cm/s/cmHg
2.4
2.6
2.8
3.0
3.2
3.4
1000/T, K^{-1}
LU-11

(11)

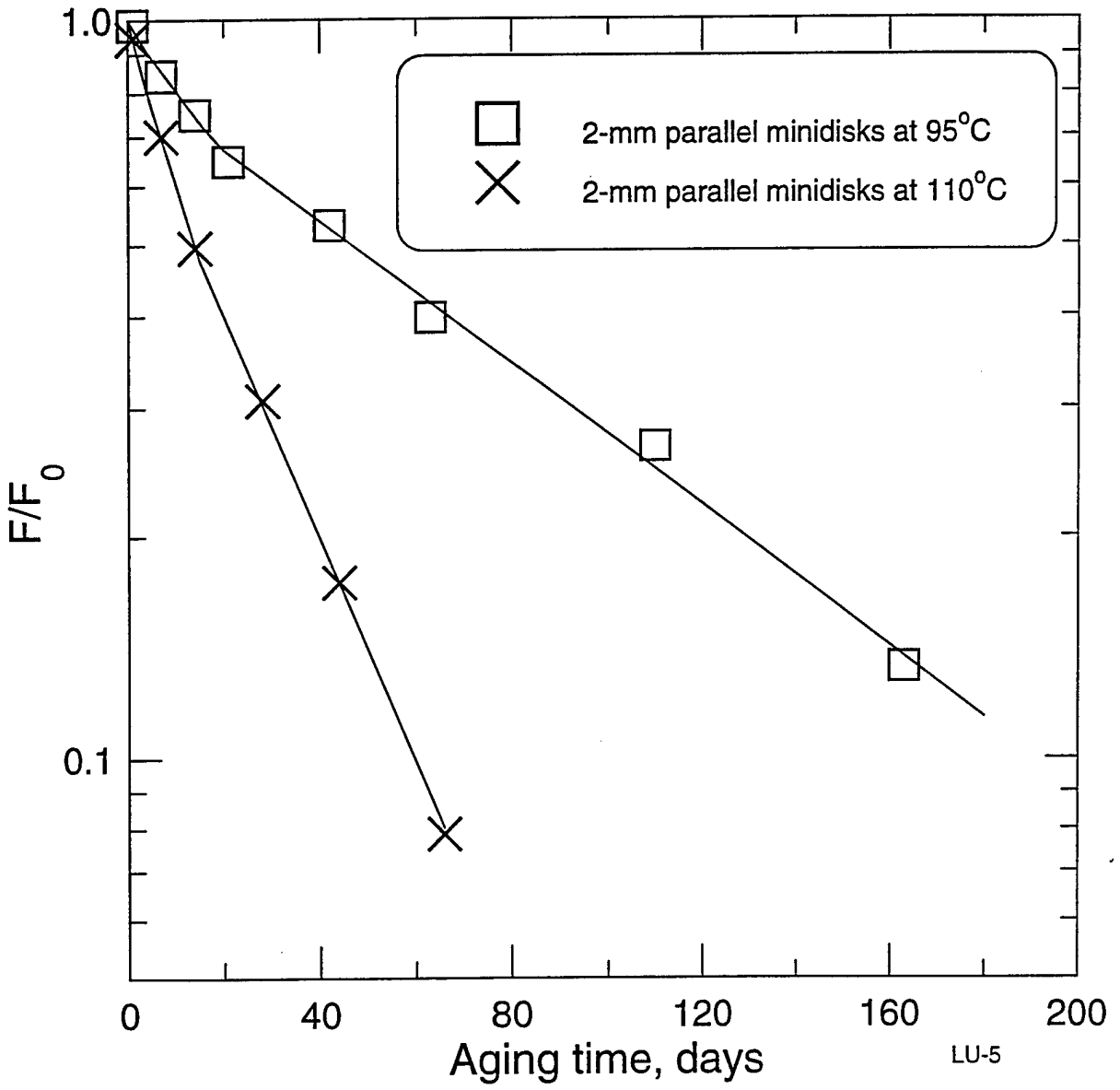
1.0
0.1
F/F0
2-mm parallel minidisks at 95°C
2-mm parallel minidisks at 110°C
0
40
80
120
160
200
Aging time, days
LU-5

(12)

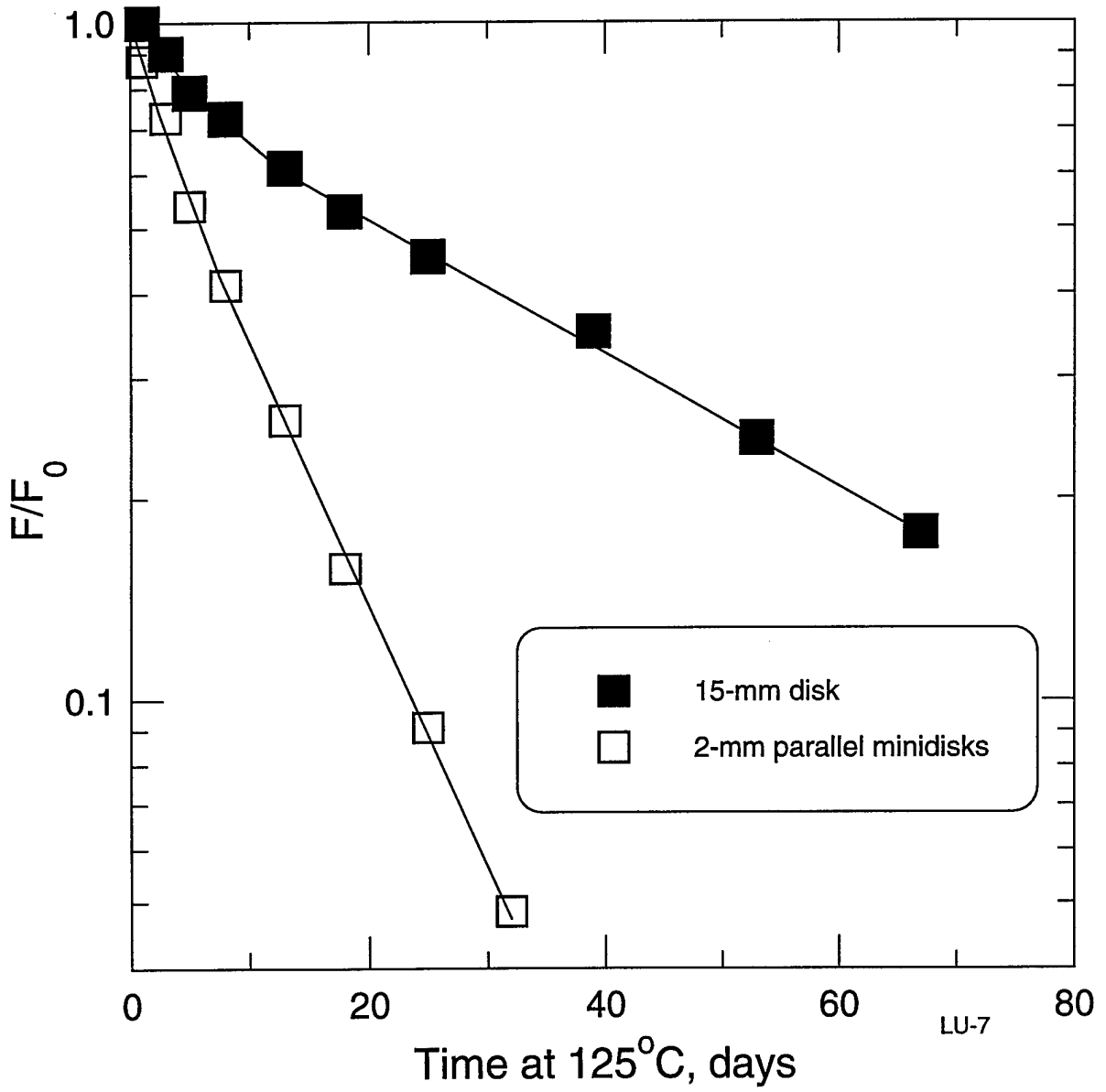
1.0
0.1
F/F0
0
20
40
60
80
Time at 125°C, days
15-mm disk
2-mm parallel minidisks
LU-7

13

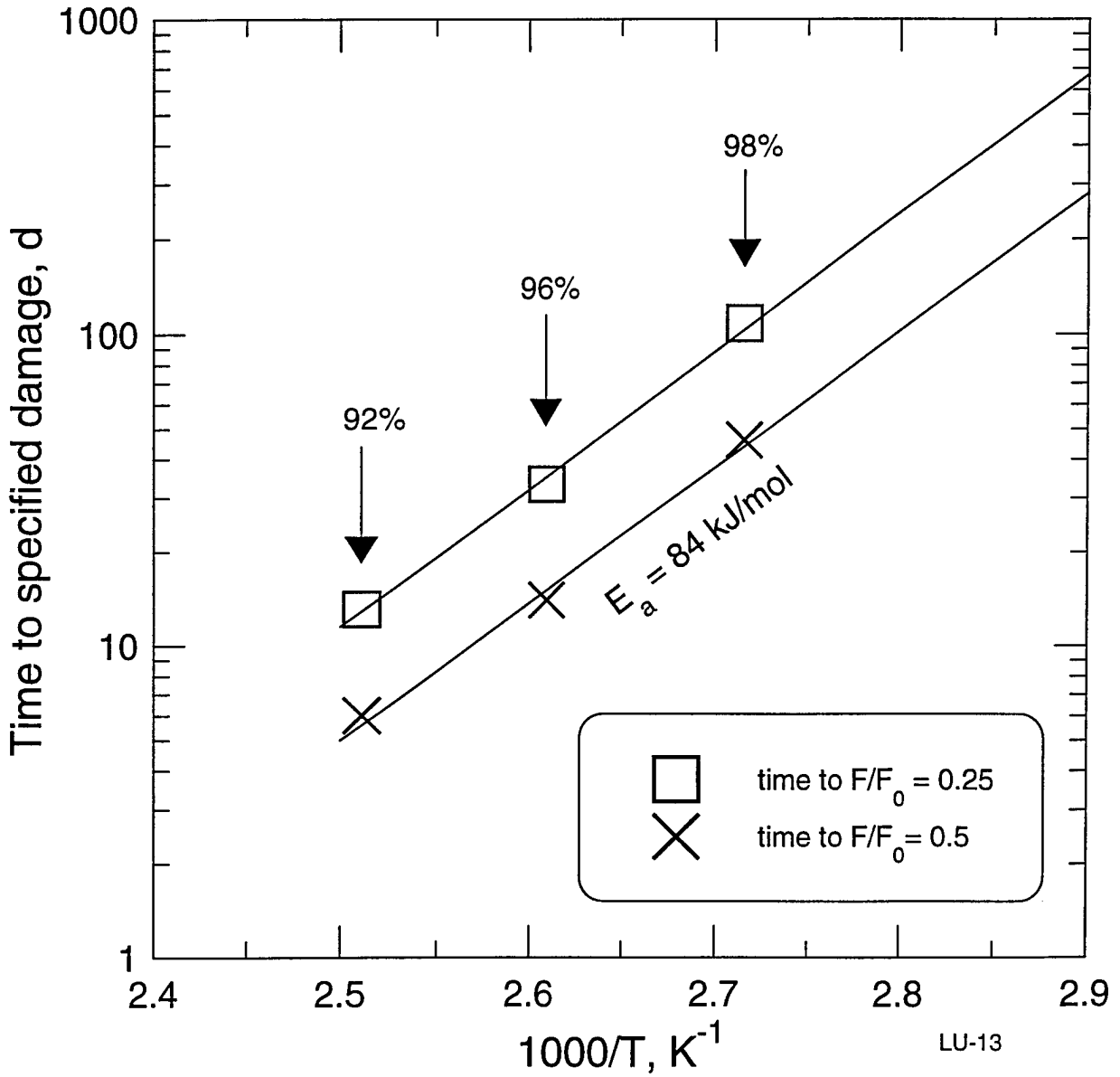
1000
100
10
1
Time to specified damage, d
98%
96%
92%
E_a = 84 kJ/mol
time to F/F_0 = 0.25
time to F/F_0 = 0.5
2.4
2.5
2.6
2.7
2.8
2.9
1000/T, K^{-1}
LU-13

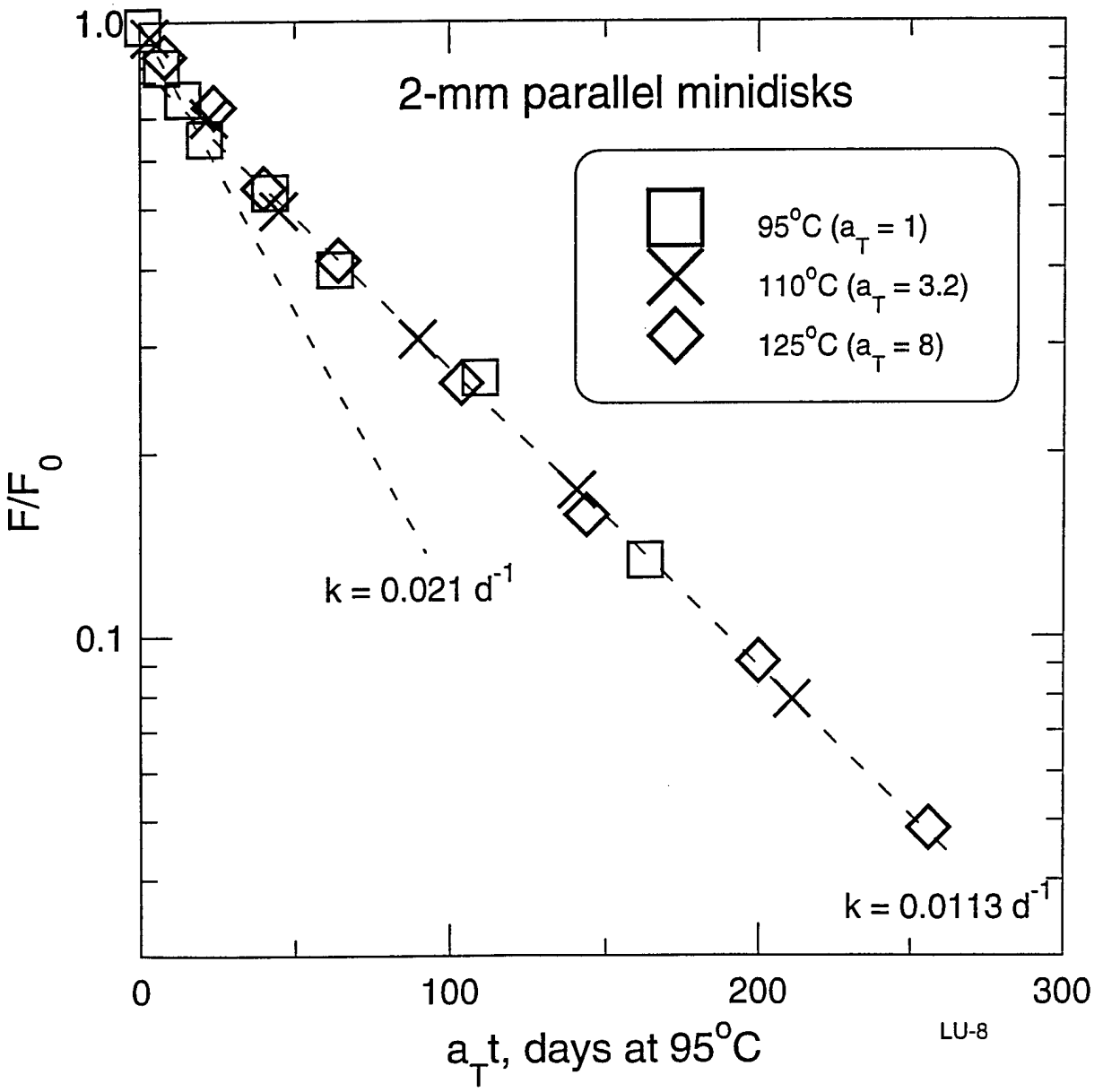
2-mm parallel minidisks
95°C (a_T = 1)
110°C (a_T = 3.2)
125°C (a_T = 8)
k = 0.021 d^-1
k = 0.0113 d^-1
F/F_0
1.0
0.1
0
100
200
300
a_T t, days at 95°C
LU-8

15

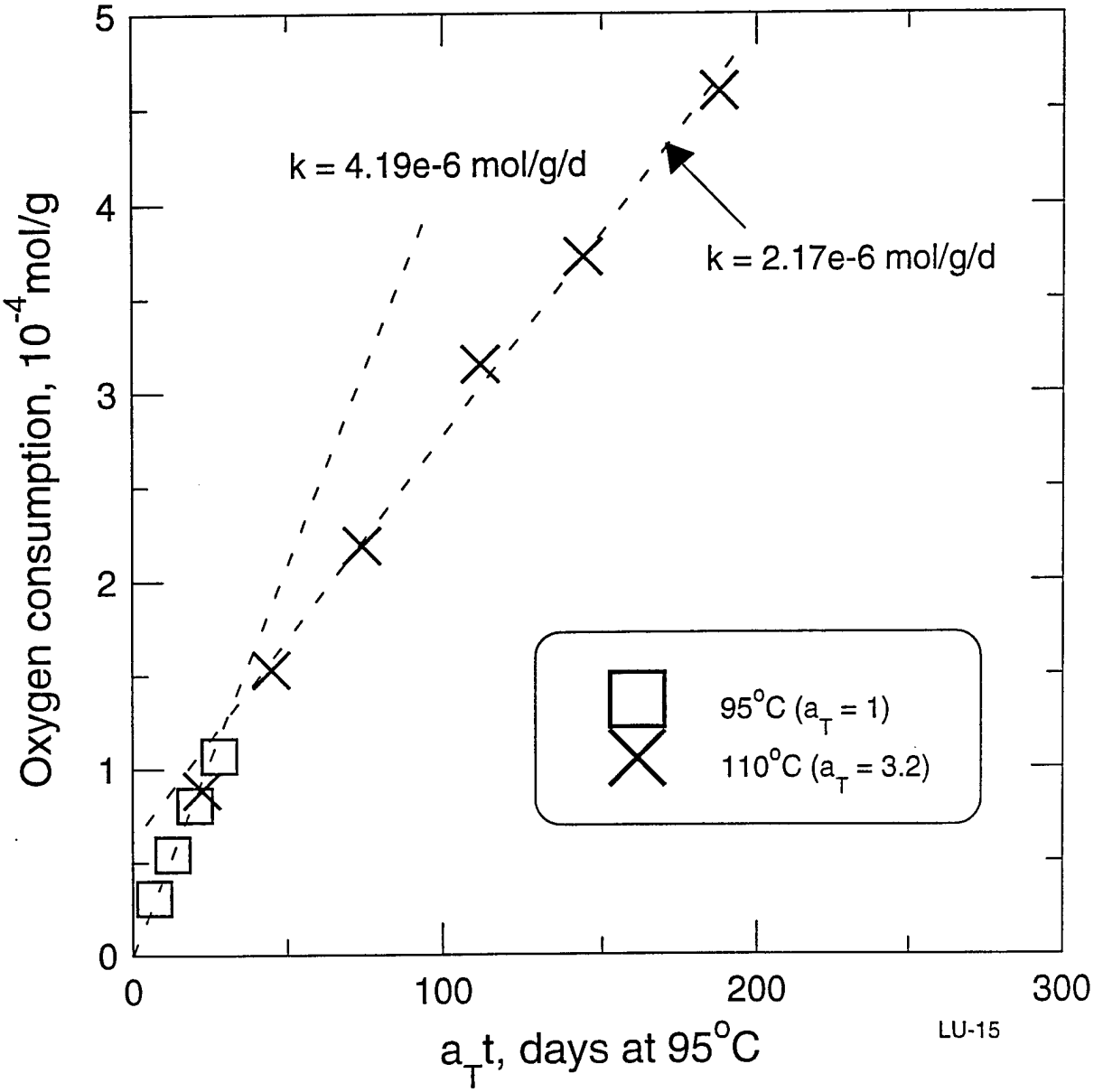
k = 4.19e-6 mol/g/d
k = 2.17e-6 mol/g/d
95°C (a_T = 1)
110°C (a_T = 3.2)
Oxygen consumption, 10^-4 mol/g
a_T t, days at 95°C
0
1
2
3
4
5
0
100
200
300
LU-15

Report Number (14) SAND--98-0854C
CONF-980642---

Publ. Date (11) 199806
Sponsor Code (18) DOE/DP, XF
UC Category (19) UC-700, DOE/ER

DOE